



## Localized Instability on the Route to Disorder in Faraday Waves

Itamar Shani, Gil Cohen, and Jay Fineberg

*The Racah Institute of Physics, The Hebrew University of Jerusalem, Jerusalem 91904, Israel*

(Received 8 December 2009; published 7 May 2010)

We experimentally investigate how disorder comes about in parametrically excited waves on a fluid surface (Faraday waves). We find that the transition from an ordered pattern to disorder corresponding to “defect-mediated turbulence” is mediated by a spatially incoherent oscillatory phase. This phase consists of highly damped waves that propagate through the effectively elastic lattice defined by the pattern. They have a well-defined frequency, velocity, and transverse polarization. As these waves decay within a few lattice spaces, they are spatially and temporally uncorrelated at larger scales.

DOI: [10.1103/PhysRevLett.104.184507](https://doi.org/10.1103/PhysRevLett.104.184507)

PACS numbers: 47.54.-r, 05.45.-a, 47.27.Cn, 64.60.Cn

Many driven spatially extended nonlinear systems become unstable to ordered patterns. As the driving is increased, these ordered structures typically break down to complex and highly disordered states [1]. Understanding the transition from order to disorder remains a central challenge in the study of nonlinear systems.

The Faraday system, in which a thin layer of fluid is subjected to spatially uniform vertical vibration, is commonly used as a model system when investigating pattern formation [2]. When driven well beyond the threshold for pattern formation, the ordered patterned structure is lost. The type of spatial disorder observed in this system, coined “defect-mediated turbulence” (DMT) [3], occurs in a wide class of driven nonlinear systems [4–6]. DMT is well characterized [4–6]; beyond a critical value of the driving, defects (dislocations of pattern lines) spontaneously nucleate throughout the system, their nucleation rate increases with the driving, and their motion generates rapid exponential decay of temporal and spatial correlations.

In many such systems, oscillatory fluctuations in the region between the ordered and DMT states have been observed, but not clearly characterized. Long wavelength modulations of square patterns in the Faraday system occurred jointly with defect nucleation [4] and fluctuations of a soft longitudinal mode in tilted rolls played an essential part in the transition to DMT in electroconvection [7]. DMT in torsional Couette flow [8] was also preceded by pattern oscillations. Finally, a secondary instability to coherent oscillatory modes preceded a “melting” transition of square patterns in a granular gas [9].

Utilizing the Faraday system, we will describe a new pathway to disorder, the oscillatory transition phase (OTP), in which the transition to DMT is mediated by a well-defined phase instability. We will show that the OTP corresponds to excited elastic waves in a lattice. These waves are highly damped and uncorrelated spatially, yet have a well-defined polarization, propagation velocity, and frequency.

The system was driven by a spatially uniform acceleration of the form  $A \sin(2 \times 2\pi\Omega t)$ . At a critical acceleration,  $A_c$ , standing waves of frequency  $\Omega$  corresponding to

wave number,  $k$ , are excited. We define our control parameter as  $\varepsilon = (A - A_c)/A_c$ .

The experimental system consists of two immiscible fluid layers enclosed within a circular 150 mm diameter cell that was bounded from above by an optical window and from below by a mirrored surface. The lower fluid was a  $h = 1.75$  mm deep aqueous solution of sodium polytungstate and dye (Fast Green FCF) of kinematic viscosity  $\nu = 1.95$  cSt and density  $\rho = 1.6$  g/cm<sup>3</sup>. The upper fluid layer was transparent silicone oil ( $\nu = 100$  cSt,  $\rho = 0.96$  g/cm<sup>3</sup>) of depth 8.25 mm. The sodium polytungstate concentration was set to match the refractive index,  $n$ , of the silicone oil, at a temperature of  $T = 28.5$  °C to an accuracy of  $\Delta n = 0.001$ . Our experiments were in a highly dissipative regime as  $\sqrt{\nu/\Omega h^2} > 0.2$ .

We use light absorption to measure the height of the waves that are excited along the surface separating the two fluids [10]. The fluid interface height was imaged at each spatial point by illuminating the entire cell by collimated monochromatic light, directed normal to the cell. The beam was reflected back through the system and imaged by a CCD camera. As lensing was prevented by index-matching the fluids, the beam’s intensity was exponentially dependent on the depth of the lower (absorbing) layer at each spatial point. Thus, the logarithm of the beam intensity at each point provided a precise linear measure of the corresponding fluid height.

Experiments performed at three response frequencies  $\Omega = 16, 18, 21$  Hz (with respective values  $A_c = 7.25, 8.65, 11.3$  g) produced qualitatively similar results. In each experiment  $\Omega$  was set and  $\varepsilon$  was gradually increased. Upon each increase of  $\varepsilon$ , we waited 10 minutes for the system to stabilize before acquiring 1200–2000 sequential images of the pattern. Image acquisition was performed at intervals of  $\Omega^{-1}$ , at the phase of the maximal wave amplitude. Unless otherwise noted, all time and length scales will be presented in units of  $T = \Omega^{-1}$ , and pattern wavelength (lattice spacing),  $a \equiv (2\pi)/k$ .

Figure 1 shows an overview of the different phases within the system. As  $\varepsilon$  is increased, the system progresses from an ordered [Fig. 1(a)] square patterned phase con-

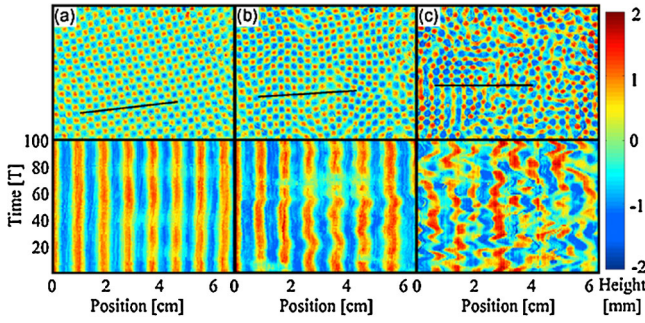


FIG. 1 (color online). Overview of system behavior with increasing  $\varepsilon$  at  $\Omega = 21$  Hz. Images of typical patterns (top) with corresponding temporal profiles of surface heights (bottom). The black lines of length 6.5 cm denote the locations where the temporal profiles were acquired. (a)  $\varepsilon < 0.32$  square patterns are stable with rare defects. (b)  $0.32 < \varepsilon < 0.5$  OTP, patterns deform via oscillations within the lattice. (c)  $\varepsilon > 0.66$  DMT. Defect numbers increase abruptly, breaking the pattern into domains. Lattice point motion increases in amplitude and becomes temporally irregular.

taining a few sporadic defects to a disordered DMT phase [Fig. 1(c)]. The OTP is a transition phase characterized by oscillatory motion of the peak surface-wave locations [Fig. 1(b)]. In this phase, defect density remains low.

What is the nature of the OTP? Secondary instabilities of striped patterns of Faraday waves in a highly viscous fluid [11] were described as an amplitude modulation, whereas in low viscosity fluids [12] square patterns become unstable to phase modulations corresponding to motion of defects. To address this question, we characterize the pattern as a lattice of points,  $\mathbf{r}_n(t)$ , denoting the surface-wave peaks, where  $n$  is the index of each lattice point. Analysis of the  $n$ -averaged temporal spectra of the surface elevation at each lattice point  $n$  [Fig. 2(a) inset] rules out an amplitude instability as no coherent amplitude modulations are observed.

To examine the dynamics of the pattern's phase, we consider the set of displacement vectors,  $\mathbf{u}$ , calculated at each lattice point  $n$ :  $\mathbf{u}_n(t) = \mathbf{r}_n(t) - \mathbf{r}_n(t_0)$ , where  $t_0$  is an arbitrary initial time. Spatial gradients of the displacement field can be estimated by displacement differences between neighboring lattice points:  $\Delta \mathbf{u}_{mn} = \mathbf{u}_m - \mathbf{u}_n$ , where  $m, n$  are indices of nearest-neighbor lattice points.

We now characterize the lattice vibrations by considering the spectrum  $\Delta u(f)$  of the displacement differences  $\Delta \mathbf{u}_{mn}$ .  $\Delta u(f)$  is calculated in Eq. (1) by Fourier transforming each of the  $x, y$  components of  $\Delta \mathbf{u}_{mn}$ , averaging the absolute value of the result over all nearest neighbors  $m, n$  and summing over both spatial components:

$$\Delta u(f) = \sqrt{\langle [\Delta u_{mn}(f)]_x \rangle_{m,n}^2 + \langle [\Delta u_{mn}(f)]_y \rangle_{m,n}^2}. \quad (1)$$

Figure 2(a) shows that the spectrum of vibrations is  $\varepsilon$  invariant at low driving amplitude, but beyond  $\varepsilon_{\text{otp}} = 0.32$  the amplitude of a narrow band of frequencies grows with

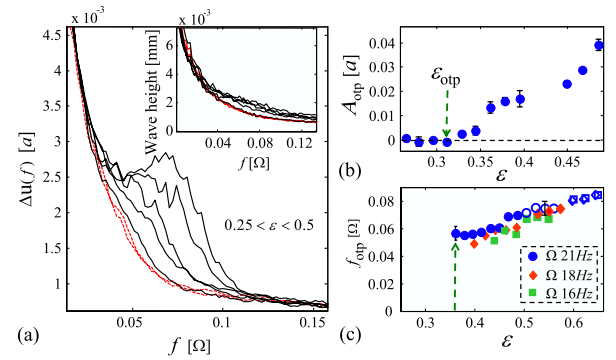


FIG. 2 (color online). The OTP as a phase instability. (a) The Fourier spectra,  $\Delta u(f)$ , are independent of  $\varepsilon$  for low  $\varepsilon$  (light lines,  $\varepsilon < 0.32$ ). At higher values of  $\varepsilon$ , vibration amplitudes increase within a narrow range of frequencies (dark lines). (Inset) Spectra of surface-wave heights of the same experiments are  $\varepsilon$ -independent, indicating that the oscillations are a phase instability. (b)  $A_{\text{otp}}$  as a function of  $\varepsilon$ .  $A_{\text{otp}}$  is defined as the integrated amplitude of the spectra in (a) after subtraction of the low  $\varepsilon$  background spectra [light lines in (a)].  $A_{\text{otp}} > 0$  defines the transition to OTP at  $\varepsilon = \varepsilon_{\text{otp}}$ . Data in (a) and (b) are for  $\Omega = 21$  Hz. (c) The peak frequency,  $f_{\text{otp}}$ , of  $\Delta u(f)$  is finite at onset and increases linearly with  $\varepsilon$ . Full (open) symbols denote measurements in the OTP (DMT phase). When normalized by  $\Omega$ , the oscillation frequency curves collapse. Error bars are representative for all measurements in (c).

$\varepsilon$ . This indicates that the OTP indeed corresponds to a phase instability.

We can now quantify the vibration amplitude. We first note that, except for the band of frequencies excited by the instability,  $\Delta u(f)$  does not vary with  $\varepsilon$ . We define the vibration amplitude,  $A_{\text{otp}}$ , as the integrated amplitude of  $\Delta u(f)$  after subtracting the background spectrum obtained for  $\varepsilon < 0.32$ .  $A_{\text{otp}}$  is both a time- and space-averaged quantity. Figure 2(b) shows that, beyond a critical value,  $\varepsilon = \varepsilon_{\text{otp}}$ ,  $A_{\text{otp}}$  grows in an approximately linear fashion with  $\varepsilon$ . This is true for all values of  $\Omega$  tested. Linear extrapolation of  $A_{\text{otp}}$  to zero yields the OTP onset,  $\varepsilon_{\text{otp}}$ .  $\varepsilon_{\text{otp}}$  slightly varied with  $\Omega$  with respective values of  $\varepsilon_{\text{otp}} = 0.33, 0.37, 0.32 \pm 0.03$  for  $\Omega = 16, 18, 21$  Hz. As shown in Fig. 2(c), the peak frequency of the instability,  $f_{\text{otp}}$ , is finite at onset and increases linearly with  $\varepsilon$ , therefore suggesting that the instability has the character of a Hopf bifurcation. As Fig. 2(c) indicates, the oscillation frequency curves superimpose, when scaled with  $\Omega$ .

To this point, our description of the pattern as a lattice was simply a convenient way to characterize the OTP. Can this analogy to a lattice in an elastic medium be pushed further? This approach was successfully used by Goldman *et al.* [9] to describe pattern dynamics of a parametrically excited granular gas. In an elastic medium, distortions of the lattice displacement field  $\mathbf{u}$  should propagate through the lattice as elastic waves with two possible polarizations—transverse,  $\nabla \times \mathbf{u}$ , and longitudinal,  $\nabla \cdot \mathbf{u}$ . To cal-

culate these quantities, we perform spatial differentiation of  $\mathbf{u}$  by taking differences of  $\mathbf{u}$  at neighboring lattice points in predefined directions,  $x, y$ .

The spectra of  $\nabla \times \mathbf{u}$  and  $\nabla \cdot \mathbf{u}$ , averaged over all lattice points, are presented in Figs. 3(a) and 3(b). Whereas the  $\nabla \cdot \mathbf{u}$  spectra do not vary with  $\varepsilon$  [Fig. 3(b)], a peak indeed appears in  $\nabla \times \mathbf{u}$  for  $\varepsilon > \varepsilon_{\text{otp}}$  [Fig. 3(a)]. Thus, the instability has a well-defined transverse polarization.

If the analogy to lattice excitations is relevant, we should also expect these ‘‘lattice waves’’ to propagate at a well-defined velocity. To measure this velocity, we cross correlate temporal signals of  $\nabla \times \mathbf{u}$  at spatially separated lattice locations. In Fig. 3(c) we present the cross-correlation amplitudes, when averaged over all pairs of lattice sites that are separated by a distance  $d$  along any of the two lattice directions. The figure shows that the peak cross-correlation values occur at times,  $\Delta t$ , that increase linearly with  $d$ . The slope of the  $d$  vs  $\Delta t$  curves provides us with the velocity of these transverse lattice waves, yielding a propagation velocity of  $c_{\text{otp}} = 0.6$  for the data in Fig. 3(c). Figure 3(d) surprisingly demonstrates that this velocity is constant in both  $\varepsilon$  and  $\Omega$ . Thus, the propagation velocity,  $c_{\text{otp}}$ , of these lattice waves is a well-defined quantity which is, in a sense, a characteristic ‘‘material’’ property of the lattice.

Figure 3(c) also shows that these waves rapidly decay, approximately exponentially, as a function of their

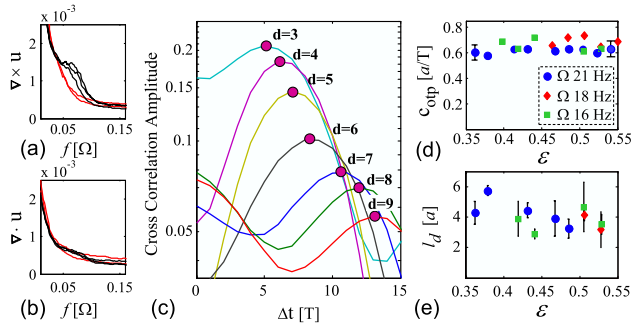


FIG. 3 (color online). Characterization of the OTP lattice waves. Peaks appear for  $\varepsilon > \varepsilon_{\text{otp}}$  solely in the temporal spectra of  $\nabla \times \mathbf{u}$  (a), while the temporal spectra of  $\nabla \cdot \mathbf{u}$  (b) are unaffected. The  $\nabla \times \mathbf{u}$  oscillations are associated with transverse waves. Light lines are measurements at the stable phase,  $\varepsilon = 0.29, 0.31$ . Dark lines are measurements after OTP onset,  $\varepsilon = 0.45, 0.47, 0.49$ .  $\Omega = 21$  Hz. (c) Mean temporal cross-correlation amplitudes of  $\nabla \times \mathbf{u}$  at increasing distances  $d$  along lattice lines ( $\Omega = 21$  Hz,  $\varepsilon = 0.47$ ). The correlations peak at times linearly growing with  $d$ . The peak amplitudes decay exponentially with  $d$ . Cross correlations were obtained using time series whose duration was much longer than  $1/f_{\text{otp}}$ , and results were averaged over all lattice points. Wave velocities (d) and attenuation lengths (e) as a function of  $\varepsilon$  and  $\Omega$ . Velocities (decay lengths) were extracted by linear (exponential) fits to the correlation peak time (amplitude) vs distance. Wave velocities were independent of both  $\varepsilon$  and  $\Omega$ .

propagation distance. The decay lengths,  $l_d$ , are shown in Fig. 3(e) as a function of both  $\varepsilon$  and  $\Omega$ . The OTP waves are strongly damped and effectively disappear after 3 to 6 lattice spacings. The wavelength,  $c_{\text{otp}}/f_{\text{otp}} \sim 10$ , is longer than the attenuation length. This over-damped nature is why these lattice waves are so highly localized.

We now consider the transition to the DMT phase. The defect density in the lattice is defined as the ratio between the time-averaged number of defects and the total number of lattice site pairs in a perfect square lattice. As Fig. 4(a) shows, defect densities, which were low in both the stable and OTP phases, sharply increase at a well-defined threshold,  $\varepsilon_d = 0.6, 0.56, 0.495 \pm 0.01$ , for  $\Omega = 16, 18, 21$  Hz. This increase in defect density destroys spatiotemporal correlations within the lattice. This is demonstrated in Fig. 4(a), where the transition to DMT is accompanied by a sharp drop of the coherence time, defined as the time for which the surface height autocorrelation function drops to half of its initial value. One might think that the oscillation amplitudes would be damped by this sharp drop in lattice coherence, but, as Fig. 4(b) demonstrates, the opposite actually occurs as  $A_{\text{otp}}$  increases sharply.

The relation between defects and waves may be, in a sense, symbiotic. Sporadic defects are always present in our system due to the frustration between the circular

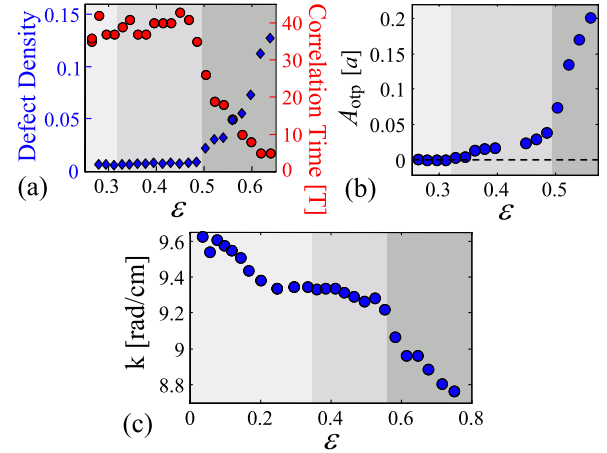


FIG. 4 (color online). The transition to DMT and wave number selection. Phases, denoted by shading, are (from left to right): stable, OTP, and DMT. (a) Defect density (diamonds) and correlation time (circles) as a function of  $\varepsilon$ .  $\Omega = 21$  Hz. Beyond  $\varepsilon = \varepsilon_d$ , defect density sharply increases. In parallel, correlation times drop sharply. This shows clearly that the defects are the source of both spatial and temporal disorder. Correlation times are defined by the times where the autocorrelation function of the surface elevation  $h(x, y, t)$  equals  $\frac{1}{2}$ . Both correlation times and defect density show little change for  $\varepsilon < \varepsilon_d$ . (b) The linear growth of the instability vibration amplitude,  $A_{\text{otp}}$ , terminates at  $\varepsilon = \varepsilon_d$  with a sharp increase.  $\Omega = 21$  Hz. (c) The time-space-averaged wave number,  $k$ , as a function of  $\varepsilon$  for  $\Omega = 36$  Hz.  $k$  decreases during both the stable and DMT phases and is nearly constant throughout the OTP.

lateral boundaries and the square pattern [13]. Despite their continual presence, defects are not the cause of the OTP instability, since a well-defined threshold,  $\varepsilon_{\text{otp}}$ , exists for the onset of lattice vibrations. Although not the sole source for lattice wave initiation, the proximity of a defect may provide a sufficiently strong perturbation to trigger a lattice wave. This is due to the curving of lattice lines around the defect cores as they move. On the other hand, large-amplitude lattice waves could well provide a sufficiently large perturbation to trigger the nucleation of a defect [4,9]. In the DMT phase, Figs. 4(a) and 4(b) indicate that  $A_{\text{otp}}$  increases significantly with defect density. Thus, a synergistic “feedback” between defects and lattice waves could provide an explanation for the rapid nucleation of defects that defines the DMT phase.

Because of defect nucleation and motion, local pattern wave numbers generally vary in time and space within all of the phases. The mean wave number,  $k$ , is, however, well-defined. Figure 4(c) describes how  $k$  varies with  $\varepsilon$ . Throughout most of the stable phase,  $k$  decreases continuously. This decrease is consistent with a nonlinear frequency or wave number shift with  $\varepsilon$ . Within the DMT phase,  $k$  continues to decrease with  $\varepsilon$  at about the same rate as in the ordered phase. Surprisingly, the wave number decrease ceases at  $\varepsilon \sim 0.8\varepsilon_{\text{otp}}$ , and remains fairly constant throughout the entire OTP. This result may provide a mechanism of the system’s phase transitions, if we assume that the decrease of  $k$  with  $\varepsilon$  represents an “equilibrium” wave number. Then, in analogy to an elastic solid, the plateau in  $k$  throughout the OTP suggests an imposed mechanical “strain,” which increases with the distance of  $k$  from its equilibrium value. Real crystalline materials yield under imposed strain by the nucleation of defects in the lattice structure, with the defect density increasing with strain. Analogous behavior may be happening when the ordered lattice state transitions to the DMT phase. The analogy to crystalline dynamics driven by strain-induced disorder could potentially yield new insights into both the nature and characterization of a wide range of driven nonlinear systems.

We have described a new type of instability in nonlinear systems that is intrinsically localized in both space and time. The highly localized nature of the waves composing the OTP implies a very low degree of phase correlation throughout the system. Thus, without an intrinsically local analysis, this instability would be difficult to identify, as analysis over larger scales would average out any correlations carried by the waves. As many qualitative similarities exist between this system and others that exhibit DMT, we surmise that these modes are quite general.

We also showed that, as in [9], the nonlinear wave pattern has some qualities analogous to those of an elastic crystalline solid. Busse showed [14] that global instabilities of ordered “crystalline” patterns in driven nonlinear systems can be described by Bloch-type analysis. Whether this approach can describe the highly damped localized modes observed here is an open question, since the lack of phase correlation over the entire system, which destroys periodic translational symmetry, could average out signs of a global oscillatory instability.

The highly damped nature of these modes (possibly due to the dissipative nature of our lattice) suggests that a large (finite) perturbation may be needed to induce them. The mechanism giving rise to these perturbations may be related to defect nucleation and/or motion within the lattice, but understanding how or why the system selects this particular mode at a sharp threshold value of  $\varepsilon$  presents an interesting theoretical challenge.

J. F. acknowledges the support of the Max Born chair for natural philosophy.

- 
- [1] M. C. Cross and P. Hohenberg, *Rev. Mod. Phys.* **65**, 851 (1993); J. P. Gollub and J. S. Langer, *Rev. Mod. Phys.* **71**, S396 (1999); G. Ahlers, in *Dynamics of Spatio-temporal Structures—Henri Bénard Centenary Review*, edited by I. Mutabazi, J. E. Wesfreid, and E. Guyon, Springer Tracts in Modern Physics (Springer, New York, 2005).
  - [2] W. S. Edwards and S. Fauve, *Phys. Rev. E* **47**, R788 (1993); D. Binks and W. van de Water, *Phys. Rev. Lett.* **78**, 4043 (1997); H. Arbell and J. Fineberg, *Phys. Rev. Lett.* **85**, 756 (2000).
  - [3] P. Couillet, L. Gil, and J. Lega, *Physica (Amsterdam)* **37D**, 91 (1989).
  - [4] N. B. Tufillaro, R. Ramshankar, and J. P. Gollub, *Phys. Rev. Lett.* **62**, 422 (1989).
  - [5] I. Rehberg, S. Rasenat, and V. Steinberg, *Phys. Rev. Lett.* **62**, 756 (1989).
  - [6] Q. Ouyang and H. L. Swinney, *Chaos* **1**, 411 (1991).
  - [7] E. Braun, S. Rasenat, and V. Steinberg, *Europhys. Lett.* **15**, 597 (1991).
  - [8] A. Cros and P. Le Gal, *Phys. Rev. E* **70**, 016309 (2004).
  - [9] D. I. Goldman, M. D. Shattuck, S. J. Moon, J. B. Swift, and H. L. Swinney, *Phys. Rev. Lett.* **90**, 104302 (2003).
  - [10] A. V. Kityk, K. Knorr, H. W. Müller, and C. Wagner, *Europhys. Lett.* **65**, 857 (2004); T. Epstein and J. Fineberg, *Phys. Rev. Lett.* **100**, 134101 (2008).
  - [11] L. Daudet, V. Ego, S. Manneville, and J. Bechhoefer, *Europhys. Lett.* **32**, 313 (1995).
  - [12] S. Douady, *J. Fluid Mech.* **221**, 383 (1990).
  - [13] A. B. Ezersky, D. A. Ermoshin, and S. V. Kiyashko, *Phys. Rev. E* **51**, 4411 (1995).
  - [14] F. H. Busse, *Rep. Prog. Phys.* **41**, 1929 (1978).